Article

# Synthesis and Photoluminescent Properties of Size-Controlled Germanium Nanocrystals from Phenyl Trichlorogermane-Derived Polymers

Eric J. Henderson, Colin M. Hessel, and Jonathan G. C. Veinot

*J. Am. Chem. Soc.*, **2008**, 130 (11), 3624-3632 • DOI: 10.1021/ja710286a



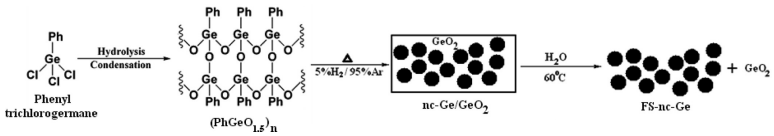


## More About This Article

Additional resources and features associated with this article are available within the HTML version:

- Supporting Information
- Links to the 1 articles that cite this article, as of the time of this article download
- Access to high resolution figures
- Links to articles and content related to this article
- Copyright permission to reproduce figures and/or text from this article

View the Full Text HTML

J|A|C|S
ARTICLES
Published on Web 02/27/2008

# Synthesis and Photoluminescent Properties of Size-Controlled Germanium Nanocrystals from Phenyl Trichlorogermane-Derived Polymers

Eric J. Henderson, Colin M. Hessel, and Jonathan G. C. Veinot*

*Department of Chemistry, University of Alberta, Edmonton, Alberta, Canada*

Received November 13, 2007; E-mail: jveinot@ualberta.ca.

***Abstract:*** We report the preparation of luminescent oxide-embedded germanium nanocrystals (Ge-NC/$GeO_2$) by the reductive thermal processing of polymers derived from phenyl trichlorogermane (PTG, $C_6H_5GeCl_3$). Sol−gel processing of PTG yields air-stable polymers with a Ge:O ratio of 1:1.5, $(C_6H_5GeO_{1.5})_n$, that thermally decompose to yield a germanium rich oxide (GRO) network. Thermal disproportionation of the GRO results in nucleation and initial growth of oxide-embedded Ge-NC, and subsequent reaction of the $GeO_2$ matrix with the reducing atmosphere results in additional nanocrystal growth. This synthetic method affords quantitative yields of composite powders in large quantities and allows for Ge-NC size control through variations of the peak thermal processing temperature and reaction time. Freestanding germanium nanocrystals (FS-Ge-NC) are readily liberated from Ge-NC/$GeO_2$ composite powders by straightfoward dissolution of the oxide matrix in warm water. Composites and FS-Ge-NC were characterized using thermogravimetric analysis (TGA), Fourier transform infrared spectroscopy (FTIR), Raman spectroscopy, X-ray powder diffraction (XRD), X-ray photoelectron spectroscopy (XPS), transmission electron microscopy (TEM), selected area electron diffraction (SAED), energy dispersive X-ray spectroscopy (EDX), and photoluminescence (PL) spectroscopy.

## 1. Introduction

The study of Group IV semiconductor nanostructures has received much attention over the past several decades, due in large part to their unique optical and electronic properties. The discovery of visible photoluminescence (PL) from silicon and germanium nanostructures[1,2] has not only challenged bulk semiconductor band structure models[3] but also significantly expanded the potential applications of these elemental semiconductors.[4] Optical applications that once seemed impossible because of the forbidden indirect band gap transition of Si and Ge may soon become reality as a result of size-induced PL. In addition, freestanding (FS) Group IV semiconductor nanocrystals have been proposed as nontoxic diagnostic and therapeutic agents.[5] These systems afford significant advances over *status quo* toxic compound semiconductor analogues that require elaborate surface passivation and encapsulation.[6] In this regard, recent reports have shown proof-of-concept application of freestanding silicon nanocrystals (FS-Si-NC) as luminescent biological probes.[7] In addition, freestanding germanium nanocrystals (FS-Ge-NC) have also been shown to exhibit photothermal conversion and serve as biomarkers for cell signaling.[8] While the interest in the optical properties of Ge nanoparticles remains strong, much attention has recently been given to the electronic properties of germanium nanostructures. Specifically, germanium nanowires have shown promise as microelectronic interconnects,[9] in large part because of the development of synthetic procedures that yield large quantities of well-defined materials.[10−13] In addition, oxide-embedded Ge-NC exhibit promising charge retention properties with potential applications in nonvolatile memory.[14−16] It is thought that the smaller band gap of Ge may provide improved data retention and write and erase speeds relative to commercially available Si-based systems.

While the optical characteristics of Si−NC have been studied extensively, Ge-NC have not been investigated in as much detail. An important difference between Si and Ge arises because of the smaller carrier effective masses and larger dielectric constant

(1) Canham, L. T. *Appl. Phys. Lett.* **1990**, *57*, 1046−1048.
(2) Yoshihito, M.; Nobuo, T.; Yoshiaki, Y.; Yoshihiko, K.; Yasuaki, M. *Appl. Phys. Lett.* **1991**, *59*, 3168−3170.
(3) Brus, L. *J. Phys. Chem.* **1986**, *90*, 2555−2560.
(4) Hirschman, K. D.; Tsybeskov, L.; Duttagupta, S. P.; Fauchet, P. M. *Nature* **1996**, *384*, 338−341.
(5) Nagesha, D. K.; Whitehead, M. A.; Coffer, J. L. *Adv. Mater.* **2005**, *17*, 921−924.
(6) Jamieson, T.; Bakhshi, R.; Petrova, D.; Pocock, R.; Imani, M.; Seifalian, A. M. *Biomaterials* **2007**, *28*, 4717−4732.
(7) Li, Z. F.; Ruckenstein, E. *Nano Lett.* **2004**, *4*, 1463−1467.
(8) Lambert, T. N.; Andrews, N. L.; Gerung, H.; Boyle, T. J.; Oliver, J. M.; Wilson, B. S.; Han, S. M. *Small* **2007**, *3*, 691−699.
(9) Wang, D.; Chang, Y. L.; Wang, Q.; Cao, J.; Farmer, D. B.; Gordon, R. G.; Dai, H. *J. Am. Chem. Soc.* **2004**, *126*, 11602−11611.
(10) Hanrath, T.; Korgel, B. A. *J. Am. Chem. Soc.* **2002**, *124*, 1424−1429.
(11) Lu, X.; Fanfair, D. D.; Johnston, K. P.; Korgel, B. A. *J. Am. Chem. Soc.* **2005**, *127*, 15718−15719.
(12) Fang, C.; Föll, H.; Carstensen, J. *Nano Lett.* **2006**, *6*, 1578−1580.
(13) Gerung, H.; Boyle, T. J.; Tribby, L. J.; Bunge, S. D.; Brinker, C. J.; Han, S. M. *J. Am. Chem. Soc.* **2006**, *128*, 5244−5250.
(14) Kanoun, M.; Busseret, C.; Poncet, A.; Souifi, A.; Baron, T.; Gautier, E. *Solid-State Electron.* **2006**, *50*, 1310−1314.
(15) Batra, Y.; Kabiraj, D.; Kanjilal, D. *Solid State Commun.* **2007**, *143*, 213−216.
(16) Beyer, V.; Von Borany, J.; Klimenkov, M. *J. Appl. Phys.* **2007**, *101*, 0945071−0945077.


**10.1021/ja710286a CCC: $40.75** 

associated with Ge.[17] As a result, interest in Ge-NC is increasing in part because it is reasonable that quantum confinement effects will emerge for larger particle sizes. It is well-known that quantum confinement-induced photoluminescence from semiconductor nanocrystals is size-dependent. Charge retention properties of oxide-embedded nanocrystals have also been shown to be strongly dependent on particle size distributions.[18] Still, the effects of nanocrystal composition and shape on these properties are poorly understood and remain the subject of active research. Hence, it is necessary to develop versatile synthetic techniques that yield materials of well-defined size, shape, and composition before the full potential of Ge-NCs can be realized and practically implemented in the aforementioned applications. Establishing such methods will also facilitate a fundamental and comprehensive understanding of size-dependent properties of Ge-NC.

To date, there has been much effort devoted to establishing robust synthetic techniques that meet these requirements. Existing methods for preparing FS-Ge-NC include solution-phase reduction of Ge(II)[19] and Ge(IV)[17,20−23] precursors, metathesis of Ge Zintl salts with $GeCl_4$,[24−26] supercritical thermolysis,[27,28] and solution-phase thermal decomposition.[29−31] Oxide-embedded Ge-NC have been prepared by chemical vapor deposition of GeO,[16,32] ion implantation[33,34] and cosputtering[2,35−40] followed by thermal annealing, sol−gel processing,[41−44] stain[45] and electrochemical[46] etching of Ge wafers, and laser-induced air breakdown processing.[47] Although these synthetic techniques have proven successful in the preparation of size-selected Ge-NC, the use of elaborate experimental infrastructure and specialized precursors limit their widespread use. In addition, challenges including limited sample sizes, broad size distributions, and contamination from residual reaction byproducts could limit the practicality of these methods. Of particular significance, it has recently been proposed that residual organic byproducts from solution-based syntheses could hinder accurate optical characterization.[48]

Reports employing substoichiometric oxides of germanium ($GeO_x$, $0 \leq x \leq 2$), germanium rich oxides (GRO), as Ge-NC precursors are surprisingly sparse throughout the literature. Analogous oxides have been studied extensively for Si (SROs) and are versatile precursors for the generation of oxide embedded Si−NC. We recently demonstrated that near-monodisperse oxide-embedded Si−NC could be prepared by reductive thermal processing of hydrogen silsesquioxane (HSQ, $Si_8O_{12}H_8$).[49,50] As with other $SiO_x$-based systems ($0 \leq x \leq 2$), these substoichiometric silicon oxides disproportionate into elemental Si and the stoichiometric oxide, $SiO_2$. There are only limited examples of $GeO_x$ films that have been prepared by magnetron cosputtering[51] and electron beam[15,52] evaporation. As is the case for their silicon-based equivalents, GROs disproportionate with appropriate thermal processing and under ideal conditions yield Ge-NC embedded in a $GeO_2$-like matrix. Although successful, these methods produced small quantities of Ge-NC and provided limited control over particle size and size distribution.

Here we report the preparation of size-controlled germanium nanocrystals embedded in germanium oxide (Ge-NC/$GeO_2$) via thermal processing of an organic functionalized germanium rich oxide obtained from the hydrolysis and subsequent condensation of phenyl trichlorogermane (PTG, $C_6H_5GeCl_3$). The reaction conditions of the present synthetic strategy were chosen to yield a GRO with a Ge:O ratio of 1:1.5, the same "metal":oxide ratio exhibited by HSQ (*vide supra*). The resulting sol−gel polymers, $(C_6H_5GeO_{1.5})_n$, obtained from the condensation of PTG, were prepared using standard laboratory techniques, and subsequent reductive thermal processing in a conventional tube furnace yielded oxide embedded Ge-NC. The presented preparative method yields near-monodisperse, oxide-embedded, luminescent nanocrystals whose size may be tailored by varying thermal processing conditions. The present approach also enables straightforward liberation of FS-Ge-NC from the surrounding oxide matrix upon exposure to warm (60 °C) water. The aqueous liberation procedure described herein yields size-controlled FS-Ge-NC bearing oxide/hydroxide surface termination.


(17) Heath, J. R.; Shiang, J. J.; Alivisatos, A. P. *J. Chem. Phys.* **1994**, *101* (2), 1607−1615.
(18) Heitmann, J.; Müller, F.; Zacharias, M.; Gösele, U. *Adv. Mater.* **2005**, *17*, 795−803.
(19) Lu, X.; Korgel, B. A.; Johnston, K. P. *Chem. Mater.* **2005**, *17*, 6479−6485.
(20) Wilcoxon, J. P.; Provencio, P. P.; Samara, G. A. *Phys. Rev. B* **2001**, *64*, 0354171−0354179.
(21) Warner, J. H.; Tilley, R. D. *Nanotechnology* **2006**, *17*, 3745−3749.
(22) Warner, J. H. *Nanotechnology* **2006**, *17*, 5613−5619.
(23) Fok, E.; Shih, M.; Meldrum, A.; Veinot, J. G. C. *Chem. Commun.* **2004**, *10*, 386−387.
(24) Taylor, B. R.; Kauzlarich, S. M.; Lee, H. W. H.; Delgado, G. R. *Chem. Mater.* **1998**, *10*, 22−24.
(25) Taylor, B. R.; Kauzlarich, S. M.; Delgado, G. R.; Lee, H. W. H. *Chem. Mater.* **1999**, *11*, 2493−2500.
(26) Taylor, B. R.; Fox, G. A.; Hope-Weeks, L. J.; Maxwell, R. S.; Kauzlarich, S. M.; Lee, H. W. H. *Mater. Sci. Eng. B* **2002**, *96*, 90−93.
(27) Lu, X.; Ziegler, K. J.; Ghezelbash, A.; Johnston, K. P.; Korgel, B. A. *Nano Lett.* **2004**, *4*, 969−974.
(28) Lu, X.; Korgel, B. A.; Johnston, K. P. *Nanotechnology* **2005**, *16*, S389−S394.
(29) Wu, H. P.; Ge, M. Y.; Yao, C. W.; Wang, Y. W.; Zeng, Y. W.; Wang, L. N.; Zhang, G. Q.; Jiang, J. Z. *Nanotechnology* **2006**, *17*, 5339−5343.
(30) Zaitseva, N.; Dai, Z. R.; Grant, C. D.; Harper, J.; Saw, C. *Chem. Mater.* **2007**, *19*, 5174−5178.
(31) Gerung, H.; Bunge, S. D.; Boyle, T. J.; Brinker, C. J.; Han, S. M. *Chem. Commun.* **2005**, 1914−1916.
(32) Gorokhov, E. B.; Volodin, V. A.; Marin, D. V.; Orekhov, D. A.; Cherkov, A. G.; Gutakovskii, A. K.; Shvets, V. A.; Borisov, A. G.; Efremov, M. D. *Semiconductors* **2005**, *39*, 1168−1175.
(33) Giri, P. K.; Kesavamoorthy, R.; Bhattacharya, S.; Panigrahi, B. K.; Nair, K. G. M. *Mater. Sci. Eng. B* **2006**, *128*, 201−204.
(34) Sharp, I. D.; Xu, Q.; Liao, C. Y.; Yi, D. O.; Beeman, J. W.; Lilienthal-Weber, Z.; Yu, K. M.; Zakharov, D. N.; Ager, J. W., III; Chrzan, D. C.; Haller, E. E. *J. Appl. Phys.* **2005**, *97*, 1243161−1243164.
(35) Takeoka, S.; Fujii, M.; Hayashi, S.; Yamamoto, K. *Phys. Rev. B* **1998**, *58*, 7921−7925.
(36) Zacharias, M.; Fauchet, P. M. *Appl. Phys. Lett.* **1997**, *71*, 380−382.
(37) Yoshihiko, K.; Hiroshi, U.; Yasuaki, M.; Yoshihito, M. *Appl. Phys. Lett.* **1992**, *61*, 2187−2189.
(38) Ninomiya, H.; Itoh, N.; Rath, S.; Nozaki, S.; Morisaki, H. *J. Vac. Sci. Technol. B* **1999**, *17*, 1903−1905.
(39) Yang, Y. M.; Yang, L. W.; Chu, P. K. *Appl. Phys. Lett.* **2007**, *90*, 0819091−0819093.
(40) Chew, H. G.; Zheng, F.; Choi, W. K.; Chim, W. K.; Foo, Y. L.; Fitzgerald, E. A. *Nanotechnology* **2007**, *18*, 1−6.
(41) Nogami, M.; Abe, Y. *Appl. Phys. Lett.* **1994**, *65*, 2545−2547.
(42) Yang, H.; Yao, X.; Wang, X.; Xie, S.; Fang, Y.; Liu, S.; Gu, X. *J. Phys. Chem. B* **2003**, *107*, 13319−13322.
(43) Yang, H.; Yang, R.; Wan, X.; Wan, W. *J. Cryst. Growth* **2004**, *261*, 549−556.
(44) Yang, H.; Yao, X.; Xie, S.; Wang, X.; Liu, S.; Fang, Y.; Gu, X.; Wang, F. *Opt. Mater.* **2005**, *27*, 725−730.
(45) Kartopu, G.; Bayliss, S. C.; Karavanskii, V. A.; Curry, R. J.; Turan, R.; Sapelkin, A. V. *J. Lumin.* **2003**, *101*, 275−283.
(46) Hee Cheul, C.; Buriak, J. M. *Chem. Commun.* **2000**, 1669−1670.
(47) Kabashin, A. V.; Magny, F.; Meunier, M. *J. Appl. Phys.* **2007**, *101*, 0543111−0543114.
(48) Gerion, D.; Zaitseva, N.; Saw, C.; Casula, M. F.; Fakra, S.; Van Buuren, T.; Galli, G. *Nano Lett.* **2004**, *4*, 597−602.
(49) Hessel, C. M.; Henderson, E. J.; Veinot, J. G. C. *Chem. Mater.* **2006**, *18*, 6139−6146.
(50) Hessel, C. M.; Henderson, E. J.; Veinot, J. G. C. *J. Phys. Chem. C* **2007**, *111*, 6956−6961.
(51) Zacharias, M.; Bläsing, J.; Löhmann, M.; Christen, J. *Thin Solid Films* **1996**, *278*, 32−36.
(52) Ardyanian, M.; Rinnert, H.; Devaux, X.; Vergnat, M. *Appl. Phys. Lett.* **2006**, *89*, 0119021−0119023.

***Table 1.*** Summary of Samples Investigated. All Samples Were Processed in Slightly Reducing Atmosphere (5% $H_2$/95% Ar)

| sample | processing temp (°C) | processing time (h) | mean crystal diameter (XRD) (nm)[a] |
|---|---|---|---|
| **1** | n/a | n/a | n/a |
| **2** | 400 | 1 | n/a |
| **3** | 500 | 1 | n/a |
| **4** | 525 | 1 | 6.2 |
| **5** | 550 | 1 | 10.3 |
| **6** | 600 | 1 | 16.3 |
| **7** | 525 | 2 | 7.9 |
| **8** | 525 | 5 | 11.5 |
| **9** | 525 | 24 | 12.7 |

[a] Values were calculated from Debye−Scherrer analysis of XRD peak broadening.

The formation, growth, and optical properties of oxide embedded Ge-NC described herein were evaluated as a function of processing time and temperature. These materials were characterized using thermogravimetric analysis (TGA), Fourier transform infrared spectroscopy (FTIR), Raman spectroscopy, X-ray diffraction (XRD), X-ray photoelectron spectroscopy (XPS), transmission electron microscopy (TEM), energy dispersive X-ray spectroscopy (EDX), selected-area electron diffraction (SAED), and photoluminescence (PL) spectroscopy.

## 2. Experimental Details

**Reagents and Materials.** Phenyl trichlorogermane ($C_6H_5GeCl_3$, 98%) was purchased from Sigma Aldrich, used as received, and stored in a nitrogen glovebox in subdued light. High-purity DI water (18.2 MΩ/cm) was obtained from a Barnstead Nanopure Diamond purification system. Isopropyl alcohol (IPA, ≥99.5%) was purchased from Fisher Scientific and used as received.

**Bulk $(C_6H_5GeO_{1.5})_n$ Polymer Preparation (1).** In a typical synthesis, 16 mL of a 65% (v/v) solution of IPA in DI water was added dropwise to 4.5 mL of $C_6H_5GeCl_3$ (7.13 g, 27.8 mmol) under inert atmosphere with vigorous stirring, using standard Schlenk techniques. The clear and colorless $C_6H_5GeCl_3$ immediately turned cloudy white as the IPA solution was added, and hydrolysis of $C_6H_5GeCl_3$ was confirmed by monitoring the pH of the reaction mixture (pH = 1). The cloudy white mixture was gently heated at 60 °C and stirred for 24 h to ensure complete condensation. The resulting white solid precipitate was isolated by vacuum filtration, washed several times with DI water, and dried *in vacuo*. The white solid product **1** (3.7 g) was obtained in yields greater than 90%, and is stable under ambient conditions.

**Bulk Ge-NC/$GeO_2$ Composite Preparation (2−9).** $(C_6H_5GeO_{1.5})_n$ polymer, **1**, was placed in a quartz reaction boat and transferred to a high-temperature tube furnace. Samples were heated to defined peak processing temperatures at 18 °C/min for predetermined times under slightly reducing atmosphere (5% $H_2$/95% Ar). The resulting solid Ge-NC/$GeO_2$ composites were obtained in yields of ca. 90% with respect to germanium content. After being cooled to room temperature, the solid composites were mechanically ground in an agate mortar and pestle. Reaction parameters and sample identification numbers are summarized in Table 1.

**Liberation of FS-Ge-NC.** FS-Ge-NC were liberated from composite **8** by dissolution of the $GeO_2$ matrix in warm water. In a typical liberation procedure, 0.04 g of **8** was stirred in 30 mL of DI water at ca. 60 °C for predetermined times ranging from 30 min to 20 h. The initial black suspension turned light brown as the reaction progressed. The FS-Ge-NC were isolated by centrifugation and washed with DI water and ethanol.

**Thermogravimetric Analysis (TGA).** TGA was performed using a Perkin-Elmer Pyris 1 TGA equipped with Pyris Thermal Analysis 7.0 software. $(C_6H_5GeO_{1.5})_n$ polymer samples were placed in a platinum pan and heated in 5% $H_2$/95% Ar from room temperature to 900 °C at 20 °C/min.

**Fourier Transform Infrared Spectroscopy (FTIR).** FTIR spectroscopy of free-flowing powders of **1**−**9** was performed using a Nicolet Magna 750 IR spectrophotometer.

**Raman Spectroscopy.** Raman spectroscopy was performed using a Renishaw inVia Raman microscope equipped with a 785 nm diode laser and a power of 3.98 mW on the sample.

**X-ray Powder Diffraction (XRD).** XRD was performed using an INEL XRG 3000 X-ray diffractometer equipped with a Cu Kα radiation source ($\lambda = 1.54$ Å). Bulk crystallinity for samples **1**−**9** was evaluated on finely ground samples mounted on a low-intensity background silicon (100) sample holder.

**X-ray Photoelectron Spectroscopy (XPS).** XPS was performed using a Kratos Axis Ultra instrument operating in energy spectrum mode at 210 W. The base pressure and operating chamber pressure were maintained at $\leq 10^{-7}$ Pa. A monochromatic Al Kα source ($\lambda = 8.34$ Å) was used to irradiate the samples, and the spectra were obtained with an electron takeoff angle of 90°. To control sample charging, the charge neutralizer filament was used during all experiments. Wide survey spectra were collected using an elliptical spot with 2 and 1 mm major and minor axis lengths, respectively, and a 160 eV pass energy with a step of 0.33 eV. CasaXPS (Vamas) software was used to process high-resolution spectra. All spectra were calibrated to the C1s emission (284.8 eV). After calibration, the background from each spectrum was subtracted using a Shirley-type background to remove most of the extrinsic loss structure. Sample compositions were determined from the emission intensities of the survey spectra using appropriate sensitivity factors.

**Transmission Electron Microscopy (TEM).** TEM, energy dispersive X-ray spectroscopy (EDX), and selected-area electron diffraction (SAED) were performed using a JEOL-2010 ($LaB_6$ thermionic emission source) electron microscope with an accelerating voltage of 200 keV. TEM samples of FS-Ge-NC were drop-coated from an ethanol suspension onto a carbon-coated copper grid.

**Photoluminescence Spectroscopy (PL).** PL spectra were evaluated at room temperature using the 325 nm line of a He−Cd laser excitation source, and emission was detected with a fiber-optic digital charge-coupled device (CCD) spectrometer whose spectral response was normalized using a standard blackbody radiator. Thin films of finely ground powders of **1**−**9** were drop-coated onto silicon wafers from an ethanol suspension. PL spectra of cloudy ethanol solutions of FS-Ge-NC were acquired in an identical manner.

## 3. Results and Discussion

We report the preparation of oxide-embedded germanium nanocrystals (Ge-NC/$GeO_2$) from the reductive thermal processing of a polymer prepared via the controlled hydrolysis and condensation of phenyl trichlorogermane (PTG, $C_6H_5GeCl_3$). Phenyl-substituted germanes are known to decompose at temperatures as low as 300 °C and have been shown to be effective precursors for germanium nanostructures.[10] The $(C_6H_5GeO_{1.5})_n$ polymer, **1**, was prepared using modified sol−gel procedures in which water and isopropyl alcohol (IPA) were added to PTG. IPA was added to the reaction solution to control the condensation of PTG by simultaneously lowering the water concentration and slowing hydrolysis rates by forming alkoxy-substituted intermediates. It was only with complete condensation that cross-linked $(C_6H_5GeO_{1.5})_n$ polymer networks possessed the targeted Ge:O ratio of 1:1.5. It is reasonable that the hydrolysis and condensation of partially cross-linked isopropoxy-substituted ($OPr^i$) phenyl germanes were catalyzed by liberated HCl and driven to completion by preferential evaporation of IPA with

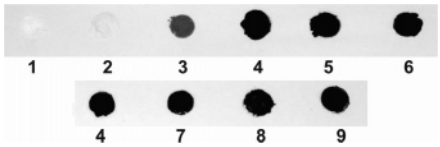


***Figure 1.*** Photographs of Ge-NC/$GeO_2$ composites thermally processed, Top: at varied peak temperatures, **1**−**6**, for 1 h, Bottom: for varied times at 525 °C, **4, 7**−**9**, noted in Table 1.

***Scheme 1.*** Schematic of (A) Hydrolysis and (B) Condensation Reactions for the Formation of **1** via Sol−Gel Processing of Phenyl Trichlorogermane (PTG) (Ph = $C_6H_5$)

**A.**

$$PhGeCl_3 + xH_2O + y(CH_3)_2CHOH \rightarrow PhGe(OH)_x(OPr^i)_y + 3HCl \quad (x + y = 3)$$

$$PhGe(OH)_x(OPr^i)_y \xrightarrow{H^+, H_2O, 60°C} PhGe(OH)_3 + y(CH_3)_2CHOH$$

**B.**

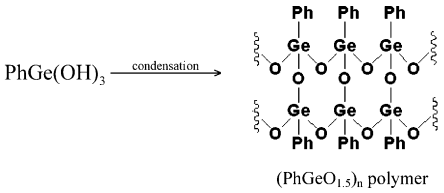


gentle heating (60 °C) and stirring for 24 h. The hydrolysis and condensation reactions for the formation of **1** from PTG are summarized in Scheme 1.

Thermal processing of **1** in 5% $H_2$/95% Ar at ≥300 °C decomposed the polymer to yield a "true" GRO with a Ge:O ratio of 1:1.5. The white solid $(C_6H_5GeO_{1.5})_n$, **1**, darkened upon thermal processing, and the color and crystallinity of the resulting composites, **2**−**9**, depended on the peak processing temperature and processing time (See Figure 1).

**Thermogravimetric Analysis (TGA).** Thermogravimetric analysis provides valuable insight into the decomposition products and a possible thermal decomposition pathway of **1**. Following the loss of residual solvent below 200 °C, thermal treatment of **1** in a slightly reducing atmosphere (5% $H_2$/95% Ar) resulted in a weight loss (ca. 38%), consistent with partial liberation of the phenyl substituents. The onset of thermal decomposition occurs at 300 °C, in agreement with previous reports of phenyl germane decomposition.[10] Coupling the TGA to a FTIR spectrometer allowed qualitative probing of the reaction byproducts and confirmed the liberation of aromatic fragments. Upon heating to higher temperatures (i.e., >700 °C), additional weight loss (ca. 5%) was observed, that we attribute to evaporation of Ge. While investigations of the reaction between $GeO_2$ and Ge at temperatures as low as 375 °C have reported the loss of volatile GeO in UHV,[53] this is unlikely for the present system at atmospheric pressure. Upon extended thermal processing (≥1 h) of bulk samples, an experimental weight loss of ca. 50% was observed, consistent with near-complete removal of the phenyl moieties and partial evaporation of Ge.

**Fourier Transform Infrared (FTIR) Spectroscopy.** Figure 2 shows the evolution of FTIR spectra with increasing peak processing temperature for samples treated for 1 h in 5% $H_2$/95% Ar, **1**−**6**. The FTIR spectrum of **1** shows characteristic

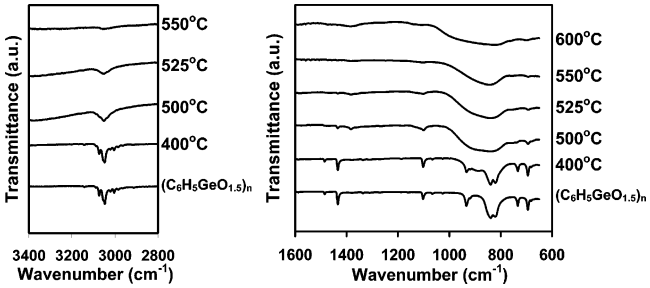


***Figure 2.*** FTIR spectra of samples **1**−**6** illustrating the influence of peak processing temperatures in 5% $H_2$/95% Ar atmosphere.

phenyl group vibrational modes, including aromatic C−H stretching at 3100−3000 $cm^{-1}$, aromatic C═C stretching at ca. 1435 $cm^{-1}$, in-plane C−H bending at ca. 1000 $cm^{-1}$, and out-of-plane C−H bending at ca. 695 $cm^{-1}$ and 735 $cm^{-1}$. The FTIR spectrum of **1** also displays intense Ge−O−Ge stretching modes at ca. 850 $cm^{-1}$, consistent with a hydrolyzed/condensed polymer.[52,54,55] The absence of hydroxyl O−H stretching at ca. 3200 $cm^{-1}$ and Ge−OH stretching at ca. 750 $cm^{-1}$ [55] confirms complete condensation of hydrolyzed PTG. Consistent with our TGA observations, increased processing temperature, **2**−**6**, was accompanied by a decrease and eventual loss of IR absorptions associated with phenyl functionalities. The evolution of the Ge−O−Ge stretching region from well-defined structured peaks to a broad featureless band is consistent with the transformation of a well-defined Ge−O structure in **1** to an extended germanium oxide network in Ge-NC/$GeO_2$ composites.[50] In addition, broadening and shifting of the Ge−O−Ge stretching mode to higher energy is consistent with the formation of germanium oxides with higher oxygen content[52] and supports the thermal transformation of "$GeO_{1.5}$" to "$GeO_2$".

FTIR spectra were monitored as a function of processing time for samples treated at 525 °C under 5% $H_2$/95% Ar, **4**, **7**−**9**. With increased processing time, the Ge−O−Ge stretching band intensity decreased until only trace absorption was observed for samples processed for 24 h, **9**. We propose this trend results from $GeO_2$ reduction by $H_2$ in the processing atmosphere, and is supported by XPS observations (*vide infra*). A gradual narrowing of the Ge−O−Ge stretching band was also observed with increased processing time, and is caused by a decreased intensity of the high-energy component of the asymmetric band (Supporting Information, S1). It is reasonable that this could result from the preferential reduction of higher oxidation state species (i.e., $GeO_2$). The role of $H_2$ in the oxide reduction and nanocrystal growth mechanism is currently being investigated in our laboratory.

**Raman Spectroscopy.** Raman spectroscopy was used to evaluate bonding in the Ge-NC core by monitoring the Ge−Ge optical phonon (OP) vibration that is centered at 302 $cm^{-1}$ for bulk crystalline Ge.[42] Figure 3A shows the evolution of baseline-corrected Raman spectra with processing temperature, **2**−**6**. Composites **2** and **3** contain no elemental germanium at the sensitivity of the Raman experiment, given the absence of the characteristic Ge−Ge OP emission. With increased processing temperature, **4**, a broad asymmetric peak emerges at ca. 294 $cm^{-1}$ which is slightly shifted to lower energy relative to bulk

(53) Prabhakaran, K.; Maeda, F.; Watanabe, Y.; Ogino, T. *Thin Solid Films* **2000**, *369*, 289−292.
(54) Zacharias, M.; Fauchet, P. M. *J. Non-Cryst. Solids* **1998**, *227*−*230*, 1058−1062.
(55) Jang, J. H.; Koo, J.; Bae, B. S. *J. Am. Ceram. Soc.* **2000**, *83*, 1356−1360.

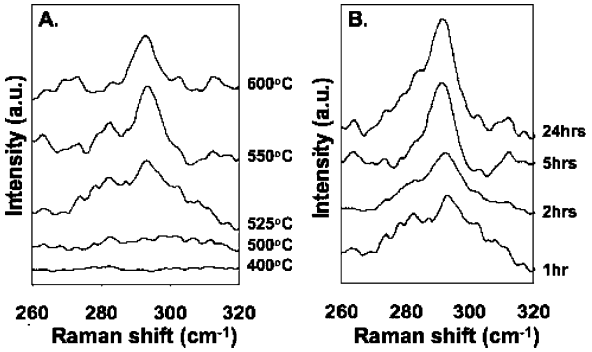


***Figure 3.*** (A**)** Baseline-corrected Raman spectra of samples **2**−**6** processed at indicated peak temperatures for 1 h in 5% $H_2$/95% Ar. (B**)** Baseline-corrected Raman spectra of samples processed for indicated times at 525 °C under 5% $H_2$/95% Ar, **4**, **7**−**9**.

Ge. The appearance of this OP vibration in the spectrum of **4** indicates Ge−Ge bonding and suggests formation of elemental germanium occurs above 500 °C. This conclusion is further supported by XRD and XPS observations (*vide infra*), and is consistent with reports on the formation of $SiO_2$-embedded Ge-NC.[44] As the processing temperature increases, **4**−**6**, the OP peak increases in intensity, narrows, and shifts to lower energy; similar trends have been attributed to Ge-NC growth.[38] The slight decrease in Ge−Ge OP intensity for samples processed at 600 °C, **6**, may be attributed to the loss of Ge through evaporation, in agreement with our TGA observations (*vide supra*).

It is generally accepted that the confinement of optical phonons in semiconductor nanocrystals results in asymmetric broadening of the OP Raman peak and a shift to lower energy relative to bulk samples.[17,34,38] As a result, the Ge−Ge OP in nanoscale systems shifts to lower energy with decreasing crystal size. This relationship has previously been used to estimate mean particle dimensions.[15,17,44] For the present study, a slight shift to lower energy is observed with increased processing temperature (Figure 3A), coincident with an increase in Ge-NC size as established by XRD (*vide infra*). While these findings may appear contradictory, similar observations have been attributed to matrix-induced compressive stresses resulting from crystal/matrix lattice mismatches.[32,34,43] As a result of the complex interplay of phonon confinement and matrix effects on the energy of the Ge−Ge OP, mean particle diameters were not determined from the present Raman data.

Figure 3B shows the evolution of baseline-corrected Raman spectra as a function of thermal processing time at 525 °C, **4**, **7**−**9**. All samples exhibit asymmetric OP emissions at lower energies than expected for bulk Ge, consistent with the presence of Ge-NC. With increased thermal processing time, the Ge−Ge OP peaks increase in intensity and narrow, consistent with nanocrystal growth.

**X-ray Diffraction (XRD).** Figure 4A shows the dependence of the X-ray diffraction pattern on peak processing temperature, **1**−**6**. The powder diffraction pattern of **1** is characterized by several broad reflections, attributed to long-range ordering in the 3D cross-linked polymer network. It is clear that processing at ≤500 °C, **2** and **3**, reduces the long-range order in **1**, yielding a noncrystalline solid. The broad feature centered at ca. $2\theta = 20°$ is characteristic of noncrystalline $GeO_2$.[56] Processing at 525 °C, **4**, generates crystalline Ge nanodomains, as evidenced by the emergence of diffraction peaks at ca. 27°, 47°, and 54° that

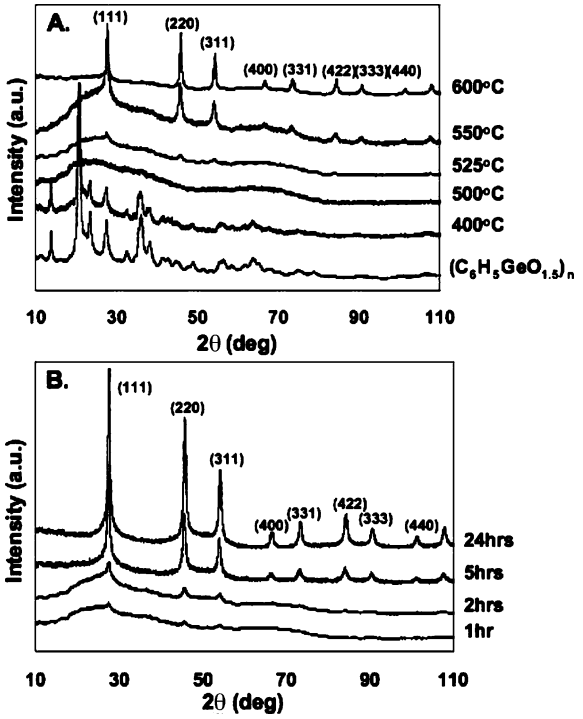


***Figure 4.*** (A**)** X-ray diffraction patterns of samples processed at indicated peak processing temperatures, **1**−**6**. (B**)** X-ray diffraction patterns of samples processed at 525 °C for various times, **4**, **7**−**9**.

are readily indexed to the (111), (220), and (311) reflections of diamond structure Ge. Following processing at higher temperatures, **5** and **6**, Ge reflections intensify and narrow, and higher order reflections corresponding to the (400), (331), (422), (333), (440), and (531) planes appear. These observations are indicative of nanocrystal growth. The Debye−Scherrer relationship was used to estimate nanocrystal size of **4**−**6** (See Table 1).

Figure 4B shows the evolution of the X-ray diffraction pattern with varied processing time at 525 °C, **4**, **7**−**9**. Increased processing time results in Ge reflections intensifying and narrowing, and the appearance of higher order reflections. As with increasing temperature, this observation is indicative of nanocrystal growth. The Debye−Scherrer relationship was used to estimate nanocrystal size as a function of processing time (see Table 1).

**X-ray Photoelectron Spectroscopy (XPS).** Figure 5A shows the evolution of the Ge 3*d* spectral region for **1**−**6**. As expected, the spectrum for **1** shows a single broad emission with a peak binding energy at ca. 32 eV, suggesting an intermediate germanium oxide species.[57] On the basis of the emission intensities of the survey spectrum of **1** and using appropriate sensitivity factors, Ge and O have relative concentrations of 1 to 1.5. This further confirms complete hydrolysis of the PTG and is consistent with our FTIR observations. In addition, there is no detectable residual Cl in the survey spectrum of **1**. XP analysis shows the appearance of a shoulder at ca. 29.5 eV for **3**−**6**, that we attribute to the presence of Ge(0). We also observe a shift of the strongest germanium oxide feature to higher binding energy (33 eV), consistent with the formation of a $GeO_2$ matrix. Similar binding energies have been obtained in XP

(56) Viswanathamurthi, P.; Bhattarai, N.; Kim, H. Y.; Khil, M. S.; Lee, D. R.; Suh, E. K. *J. Chem. Phys.* **2004**, *121*, 441−445.
(57) Molle, A.; Bhuiyan, M. N. K.; Tallarida, G.; Fanciulli, M. *Mater. Sci. Semin. Proc.* **2006**, *9*, 673−678.

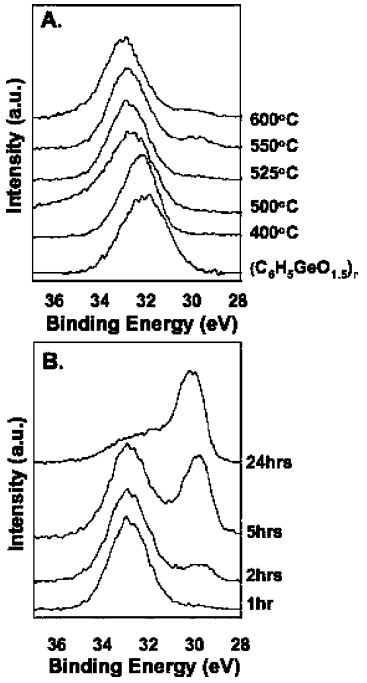


***Figure 5.*** (A) X-ray photoelectron spectra of **1**−**6** showing the thermal disproportionation of **1** into Ge and $GeO_2$. (B) X-ray photoelectron spectra of **4**, **7**−**9**, showing the thermal reduction of $GeO_2$ to Ge, and the resulting growth of Ge-NC as a function of processing time at 525 °C.

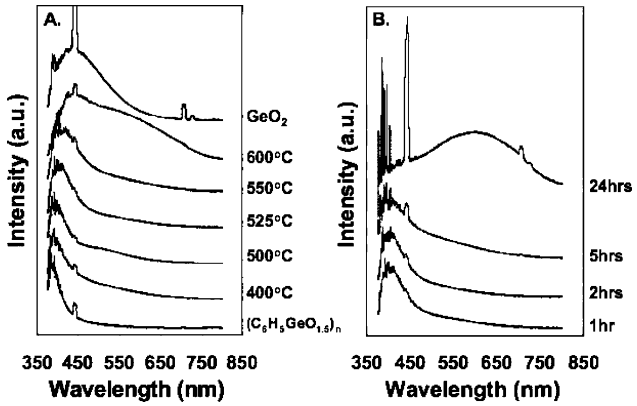


***Figure 6.*** Dependence of the photoluminescence spectra of Ge-NC/$GeO_2$ composite powders on (A) processing temperature, **1**−**6**, and (B) processing time at 525 °C, **4**, **7**−**9**. All spectra were collected with $\lambda_{ex} = 325$ nm.

analysis of other oxidized germanium nanoscale systems.[58] The evolution of the Ge(0) and Ge(IV) emissions suggests a thermally induced disproportionation reaction (i.e., $4GeO_{1.5} \rightarrow Ge + 3GeO_2$) is occurring. For the present system, the relative amount of Ge(0) increases with processing temperature, consistent with nanocrystal growth. The slight decrease in the intensity of the Ge(0) emission at 600 °C, **6**, may result from evaporation loss of elemental Ge, and agrees with present Raman and TGA observations (*vide supra*).

Figure 5B shows the evolution of the XP spectra with processing time at 525 °C, **4, 7**−**9**. Prolonged reductive thermal processing of **1** increases the concentration of Ge(0) at the expense of Ge(IV), suggesting $GeO_2$ is being reduced by $H_2$ in the processing atmosphere. The dramatic change in the amount of Ge(0) highlights that processing time may afford control of Ge-NC size. It also underscores the possibility that Ge-NC growth may be controlled by regulating the processing atmosphere composition.


***Figure 7.*** Suspensions of Ge-NC/$GeO_2$ composite in warm DI water after (A) 30 min, and (B) 20 h.

Reports describing the formation and growth of Ge-NC embedded in silica have proposed that initial reduction of $GeO_2$ (or $GeO_x$) leads to nucleation and subsequent crystal growth.[40] In contrast, for the present system we propose that following thermal decomposition of **1**, thermally induced disproportionation generates Ge(0) and Ge(IV) (i.e., $GeO_2$) from the GRO network, Scheme 2A. This process causes particle nucleation and crystal growth. If reduction of $GeO_x$ was the primary event leading to nucleation and crystal growth, as previously proposed in the literature,[40] one would expect the emission at ca. 32 eV to decrease and be replaced by a Ge(0) emission; no $GeO_2$-like species would be observed. This is clearly not the case for the present system. As a result, we propose that with prolonged heating, the $GeO_2$ matrix is reduced to Ge(0) by atmospheric $H_2$. This second source of elemental Ge provides an additional growth pathway for Ge-NC, Scheme 2B.

**Photoluminescence (PL) Spectroscopy.** As previously mentioned, the PL properties of Ge-NC are of increasing interest because quantum confinement effects are expected to appear for relatively large Ge-NC.[17] In contrast to silicon nanomaterials, the PL response of Ge-NC has not been thoroughly investigated. The size-dependent PL of Si−NC is generally accepted as a manifestation of quantum confinement.[59] It has been proposed that for nanoscale semiconductor structures with dimensions smaller than the Bohr exciton radius, confinement of charge carriers results in an enhancement of radiative recombination processes and increase in photon energy with decreasing crystal size. For Ge-NC, reports are often contradictory about the critical crystal size required for quantum confinement effects to emerge. The Bohr exciton radius for bulk Ge has been reported to be 11.5 nm,[20] 17.7 nm,[59] and 25.3 nm.[15] Further complicating a detailed understanding of the optical properties of Ge-NC, there are also numerous direct and indirect transitions that characterize bulk Ge.[17] Nevertheless, there have been numerous reports for quantum confined emission in Ge-NC, with the vast majority exhibiting size-dependent PL in the visible region of the electromagnetic spectrum.[20,25,31,32] Still, similar PL characteristics have been attributed to ultrasmall molecular-like Ge clusters, interfacial defects, surface oxides, and matrix effects.[29,36,37,43,45,52,54] Furthermore, quantum confined emission has also been reported in the NIR for Ge nanocrystals of similar

(58) Hanrath, T.; Korgel, B. A. *J. Am. Chem. Soc.* **2004**, *126*, 15466−15472.

(59) Cullis, A. G.; Canham, L. T.; Calcott, P. D. J. *J. Appl. Phys.* **1997**, *82*, 909−965.

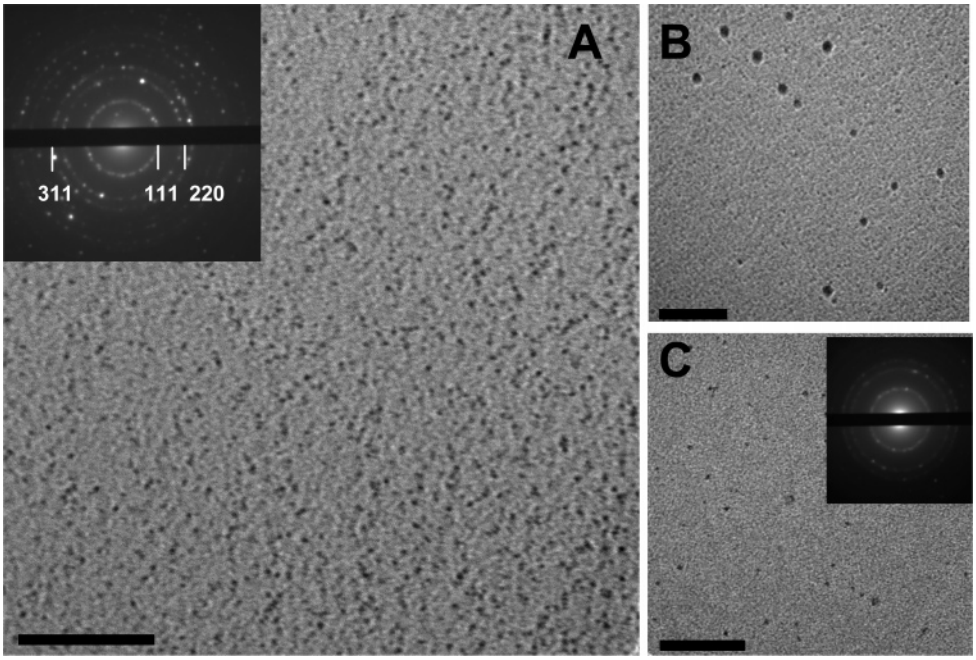


***Figure 8.*** Transmission electron micrograph of FS-Ge-NC after (A) 30 min, (B) 30 min, and (C) 2.5 h in warm DI $H_2O$. All scale bars = 100 nm. Insets: SAED patterns with indicated reflections characteristic of crystalline Ge.

***Scheme 2.*** A Schematic Representation of the Generation of Ge-NC/$GeO_2$ Composites (Ph = $C_6H_5$) (A) from the Thermal Disproportionation of Decomposed **1**, and (B) Subsequent Growth of Ge-NC from the Reduction of the $GeO_2$ Matrix by Atmospheric $H_2$

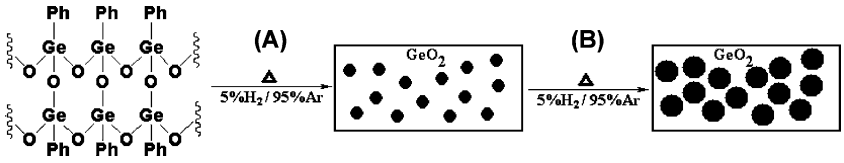


sizes.[35] From this array of examples, it is clear that the source(s) of PL emanating from Ge-NC remain the subject of some scientific controversy.

Figure 6A shows the normalized PL spectra for **1**−**6**. The sharp peak at ca. 441 nm is a spectral artifact arising from the He−Cd laser excitation source. Unprocessed **1** exhibits a sharp PL band with an emission maximum centered at ca. 390 nm. With increased processing temperature, **2**−**6**, this band broadens asymmetrically while also shifting to lower energy. The PL response of **6** shows a maximum centered at ca. 440 nm and resembles the PL behavior of amorphous $GeO_2$ (Figure 6A). We attribute this spectral feature to an oxide-mediated radiative transition, that arises either from Ge-NC surface oxide states or noncrystalline $GeO_2$ matrix. Figure 6A also shows that increased processing temperature results in the emergence of a low energy shoulder that monotonically red-shifts with increased temperature (**2**−**6**). This red-shift is consistent with quantum confined excitons in nanocrystals of increasing size, as indicated by Debeye−Sherrer analysis of XRD peak broadening, Table 1. However, in order to conclusively identify the source of this emission, detailed spectroscopic investigations, including X-ray excited optical luminescence (XEOL) spectroscopy, are actively being pursued in our group. Interestingly, upon prolonged exposure to the 325 nm laser excitation source, the "oxide" spectral feature was photobleached and the "quantum confined" component did not vary in intensity. This is consistent with reports of PL stability in semiconductor quantum dots.

Figure 6B shows the dependence of normalized PL spectra of Ge-NC/$GeO_2$ composites on thermal processing time at 525 °C, **4**, **7**−**9**. As processing time increased, the spectral feature attributed to quantum confinement in Ge-NC red-shifted, until it was completely resolved from the oxide-associated feature. Again, this is consistent with quantum-confined excitons in Ge-NC of increasing size. It can also be seen in Figure 6B that band at ca. 400 nm is of much lower intensity in the PL spectrum for **9**. This is qualitatively consistent with the loss of $GeO_2$ as established by XPS analysis (*vide supra*) and further supports our assignment of this band to an oxide-based transition.

***Scheme 3.*** Schematic Representation of the Liberation of FS-Ge-NC through the Dissolution of the $GeO_2$ Matrix in Warm DI Water

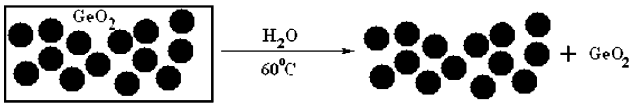


**Liberation of Freestanding Germanium Nanocrystals (FS-Ge-NC).** FS-Ge-NC were readily liberated from their oxide matrix via dissolution of $GeO_2$ in warm deionized (DI) water (ca. 60 °C). In comparison, many FS-Ge-NC synthetic methods employ toxic/corrosive etchants and elaborate purification procedures for nanocrystal liberation. For example, silica-embedded Ge-NC require hydrofluoric acid (HF),[34] and solution-based syntheses require numerous washing steps with organic solvents to free the nanocrystals from residual surfactant and other reaction byproducts.[20,25] A schematic representation of the liberation process is presented in Scheme 3.

In addition to particle liberation, we also found that prolonged exposure to DI water resulted in a gradual, controlled decrease

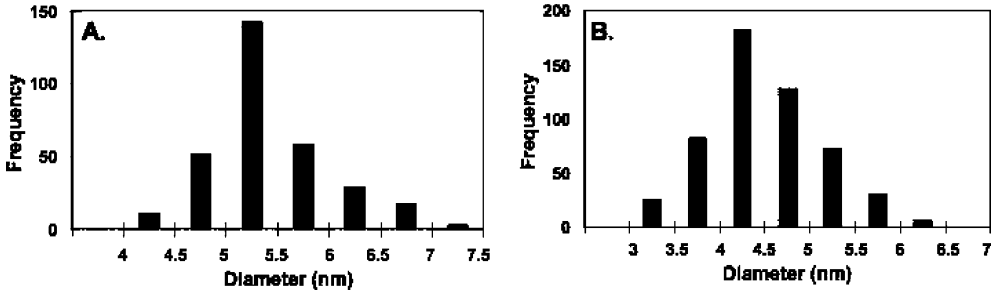


***Figure 9.*** Measured size distribution of (A) FS-Ge-NC isolated after 30 min in warm $H_2O$ (mean diameter = 5.5 nm, $n = 316$, $\sigma = 0.6$ nm), and (B) FS-Ge-NC isolated after 2.5 h in warm $H_2O$ (mean diameter = 4.5 nm, $n = 534$, $\sigma = 0.6$ nm).

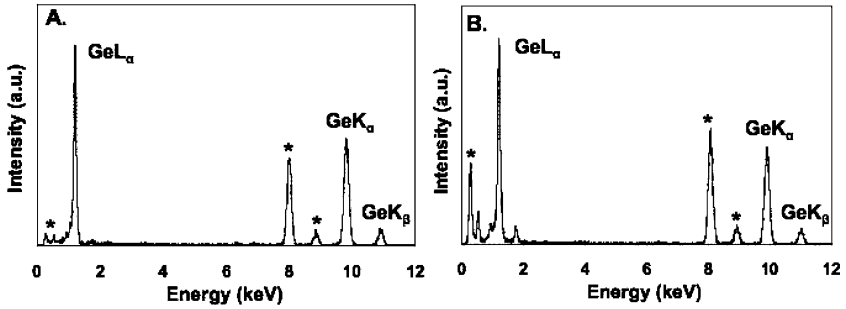


***Figure 10.*** Energy dispersive X-ray spectra of FS-Ge-NC isolated from **8** after (A) 30 min, and (B) 2.5 h, in warm $H_2O$. Peaks labeled with * are due to the TEM sample holder.

in Ge-NC size. Qualitatively, this was manifested in a change in the color of the reaction mixture from black after 30 min to light brown after 20 h (See Figure 7). We propose this results from sequential oxidation/dissolution steps, a phenomenon that has previously been reported for Ge wafers submerged in water.[60] A similar strategy that employed solutions of $HNO_3$/HF has been employed for the size tuning of Si−NC.[61] The long reaction times required for modifying the Ge-NC size with warm $H_2O$ is very beneficial, as it allows for precise control over nanocrystal dimension. A study of the mechanism of oxide dissolution and crystal size tailoring are the subject of ongoing investigation in our laboratory. The FS-Ge-NC were characterized with TEM, EDX, SAED, and PL spectroscopy.

**Transmission Electron Microscopy (TEM).** Figure 8 shows transmission electron micrographs of liberated Ge-NC isolated after 30 min and 2.5 h in warm DI water. These freestanding nanocrystals were isolated from sample **8** (i.e., **1** processed at 525 °C for 5 h in 5% $H_2$/95% Ar). Figure 8A shows the Ge-NC adopt a pseudospherical morphology and are nearly monodisperse with a mean diameter of 5.5 nm ($n = 316$, $\sigma = 0.6$ nm, Figure 9A) after 30 min in warm DI water. TEM determined nanocrystal dimensions differ significantly from those obtained by Scherrer analysis of the XRD pattern of the composite powder (11.5 nm). This difference is easily understood in the context of surface oxidation and dissolution by the aqueous environment, resulting in an overall decrease in Ge-NC size. This is supported by the observation of a small number of particles with a TEM measured diameter of ca. 12 nm, Figure 8B, consistent with XRD data. The selected-area electron diffraction (SAED) pattern of the FS-Ge-NC (Figure 8A, inset) is characteristic of diamond structure Ge and is consistent with the XRD patterns obtained for **8**. Figure 8C shows FS-Ge-NC isolated after 2.5 h in warm DI water. The nanocrystal size

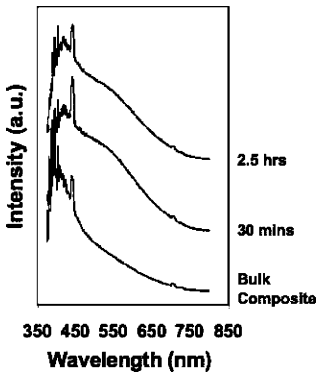


***Figure 11.*** Photoluminescence spectra of FS-Ge-NC liberated from **8** after 30 min and 2.5 h in warm $H_2O$ ($\lambda_{ex} = 325$ nm). The bottom trace is the bulk composite, **8**.

decreased as a result of longer exposure to water, having a TEM measured mean diameter of 4.5 nm ($n = 534$, $\sigma = 0.6$ nm). From the measured size distribution (Figure 9B), it is evident the particles remained nearly monodisperse. The SAED pattern (Figure 8C, inset) is consistent with diamond structure Ge and shows the nanocrystals maintain crystallinity after prolonged exposure to water. FTIR spectra of the liberated FS-Ge-NC showed oxide and hydroxide surface termination (Supporting Information, S2).

**Energy Dispersive X-ray Spectroscopy (EDX).** EDX spectra of FS-Ge-NC isolated from **8** after 30 min (Figure 10A) and 2.5 h (Figure 10B) in warm DI water indicate the nanocrystals are composed only of Ge. EDX also shows the presence of oxygen, which could be attributed to surface oxidation during sample preparation.

**Photoluminescence (PL) Spectroscopy.** Figure 11 shows the normalized PL spectra of liberated Ge-NC after 30 min and 2.5 h in warm DI water. When compared to the bulk composite powder, **8** (Figure 11, bottom trace), it is clear that the spectral feature attributed to quantum confinement (ca. 500 nm) has a

(60) Rivillon, S.; Chabal, Y. J.; Amy, F.; Kahn, A. *Appl. Phys. Lett.* **2005**, *87*, 1−3.
(61) Sato, S.; Swihart, M. T. *Chem. Mater.* **2006**, *18*, 4083−4088.

greater relative intensity in the liberated Ge-NC. This is consistent with the dissolution of the $GeO_2$ matrix by the warm water and a resulting decrease in the intensity of the oxide feature at ca. 420 nm. Figure 11 shows the PL maximum of Ge-NCs liberated after 2.5 h is slightly blue-shifted from the PL peak for the particles liberated after 30 min. This is consistent with a decrease in crystal size and further supports a quantum confined emission process.

## 4. Conclusion

We have demonstrated the preparation of oxide-embedded germanium nanocrystals (Ge-NC/$GeO_2$) from the reductive thermal processing of a polymer derived from the hydrolysis and condensation of phenyl trichlorogermane, $(C_6H_5GeO_{1.5})_n$. Following thermal decomposition of the $(C_6H_5GeO_{1.5})_n$ polymer, disproportionation of the GRO network resulted in initial Ge-NC growth, and subsequent reduction of the $GeO_2$ matrix by $H_2$ in the processing atmosphere resulted in additional crystal growth. Nanocrystal size was controlled by variations in peak processing temperature and processing time. Photoluminescence spectroscopy revealed that Ge-NC/$GeO_2$ composite powders exhibited visible emission that red-shifted with increased crystal size, suggesting quantum confined systems. Freestanding Ge-NC were readily liberated from the oxide matrix by dissolution of $GeO_2$ in warm $H_2O$, and it was found that they maintained crystallinity and PL properties. This liberation procedure also afforded crystal size control based on reaction time.

**Acknowledgment.** The authors acknowledge funding from the Natural Sciences and Engineering Research Council of Canada (NSERC), Canada Foundation for Innovation (CFI), Alberta Science and Research Investment Program (ASRIP), and University of Alberta Department of Chemistry. C. W. Moffat and R. Lister are thanked for assistance with FTIR and TGA. Prof. M. McDermott is thanked for assistance with Raman spectroscopy. Prof. A. Meldrum is thanked for access to laser systems to evaluate photoluminescence spectroscopy. The staff of the Alberta Centre for Surface Engineering and Sciences (ACSES) are thanked for XPS analysis. J. Kelly, S. McFarlane, J. Rodriguez, J. MacDonald, and D. Rollings are also thanked for useful discussions.

**Supporting Information Available:** FTIR spectra of samples **4**, **7**, **8** and FS-Ge-NC. This material is available free of charge via the Internet at http://pubs.acs.org.

JA710286A